Environmental Science & Technology

pubs.acs.org/est

Article

Distinct Roles of NO_2 versus NO and Synergisms with SO_2 in Secondary Organic Aerosol Formation from β-Myrcene Photooxidation

Ya Zhao, Chong Wang, Yingqi Zhao, Yufeng Shao, Hua Xie, Jiayue Yang, Weiqing Zhang, Guorong Wu, Gang Li,* Ling Jiang,* and Xueming Yang

Cite This: *Environ. Sci. Technol.* 2026, 60, 5097−5108

Read Online

ACCESS | Metrics & More | Article Recommendations | Supporting Information

ABSTRACT: Elucidating the impacts of gaseous pollutants on secondary organic aerosol (SOA) formation mechanisms is critical for developing effective $PM_{2.5}$ mitigation strategies. However, the combined effects of NO_x (NO_x = NO_2 + NO) and SO_2 on SOA compositions under complex photochemical conditions remain mechanistically unresolved. Here, we investigated the individual roles of NO_2/NO and their combined effects with SO_2 on β-myrcene photooxidation. Our results showed that NO_2 enhanced the SOA yield and the O:C ratio through oxidant amplification, whereas NO suppressed nucleation and oxidation states of products but facilitated particle size growth via organic nitrate partitioning. SO_2 exhibited significant synergistic effects with both NO_2 and NO, facilitating particle formation and growth processes. The newly built vacuum ultraviolet free electron laser photoionization aerosol mass spectrometer enabled the observation of a series of new compounds (i.e., organic peroxides, organic nitrate, and organosulfates) and identified new mechanisms of SOA formation. Notably, a novel compound with a molecular weight of 287 was characterized to be a nitrogen- and sulfur-containing species. These findings highlight the critical roles of pollutants in particle formation in environmental processes and provide key scientific support for regional air quality management and climate change mitigation.

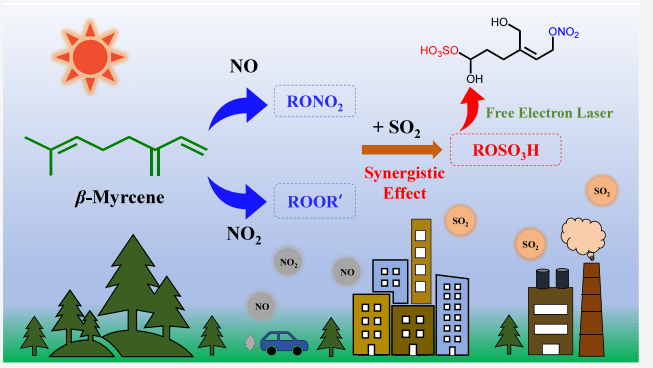

KEYWORDS: *β-myrcene, photooxidation mechanism, synergistic effect, organic nitrates, organosulfates*

1. INTRODUCTION

China's industrialization and urbanization have led to heightened energy consumption, leading to severe air pollution.[1] Although air pollutant emissions were reduced in recent years, high-pollution events where SO_2 and NO_x hourly concentrations exceed 100 ppb still frequently occur in densely populated cities.[2−6] Secondary organic aerosol (SOA) poses a major threat to both human health and air quality.[2,7,8] The processes of SOA formation are driven by photochemical reactions or oxidants, such as hydroxyl radicals (OH) and ozone (O_3).[9,10]

As one of the key pollutants, NO_x plays a critical role in regulating atmospheric oxidative capacity and alters the transformation pathways of RO_2 radicals.[11−16] Recent studies on monoterpene oxidation have revealed a general consistency in the response trends of SOA formation to NO_x concentrations; however, there were significant differences in the critical transition points ($[NO_x]_0/[VOC]_0$ (volatile organic compound)) where NO_x plays a transitional role.[16−20] Diverse research results highlighted that SOA formation was closely related to the NO_x proportion, suggesting that the composition of NO_x influences the pathways of SOA formation. Yet, the differential impacts of NO_2 and NO on the overall formation pathways of oxidation products and their component distributions remain underexplored.

Given the complexity of real-world environments, extensive studies have examined the combined effects of pollutants such as NO_x, SO_2, and NH_3, revealing significant synergistic or antagonistic effects among these components.[21−24] Notably, SO_2 not only drives new particle formation (NPF) by generating sulfate (H_2SO_4) particles but also significantly influences the chemical composition of products by enhancing acid-catalyzed reaction pathways of VOCs with appropriate humidity.[22,25−28]

Received: July 30, 2025
Revised: December 13, 2025
Accepted: January 26, 2026
Published: February 2, 2026

https://doi.org/10.1021/acs.est.5c10374
Environ. Sci. Technol. 2026, 60, 5097−5108

Table 1. Initial Experimental Conditions and Results for All β-Myrcene Photooxidation Experiments

[β-myrcene]$_0$ (ppb)	[NO_2]$_0$ (ppb)	[NO]$_0$ (ppb)	[SO_2]$_0$ (ppb)	[O_3]$_{max}$ (ppb)[a]	ΔROG (ppb)[b]	ΔM (μg/m^3)[c]	SOA yield (%)	RH (%)[d]	T (K)
408	54			26	371	315.5	15.3	2.7	296.5
404	97			61	370	460.7	22.4	1.9	296.2
403	200			144	381	690.1	32.5	2.0	296.1
401	300			202	385	939.2	43.8	2.3	296.3
389	391			221	379	930.0	44.1	0.7	295.4
407	489			278	389	1009.5	46.6	0.7	295.9
393		63		45	366	420.7	20.6	0.8	294.7
390		104		128	371	443.2	21.5	0.9	296.6
384		200		158	370	447.0	21.7	0.6	294.1
400		283		224	372	479.0	23.1	1.4	296.6
393		403		133	373	294.9	14.2	0.9	294.4
387		480		93	365	155.1	7.6	1.8	295.7
403	291		25	182	385	1465.4	68.4	0.9	294.5
410	296		56	185	390	1539.8	70.9	0.6	294.8
398	300		100	143	387	1504.5	69.8	0.7	294.7
401	299		204	160	383	1567.7	73.5	0.9	294.4
401	296		294	145	383	1593.4	74.7	1.3	294.6
412	314		393	118	396	1722.1	78.1	0.8	294.1
407		296	30	173	386	801.2	37.3	0.8	294.0
404		293	51	187	382	1032.6	48.5	0.8	294.5
413		294	105	190	387	1175.5	54.5	0.8	294.5
395		296	203	155	382	1242.4	58.4	0.9	294.2
401		301	296	150	380	1183.4	55.9	0.9	294.2
397		296	397	141	381	1094.5	51.6	0.6	294.2

[a][O_3]$_{max}$ for the maximum accumulation of O_3 in the experiments. [b]ΔROG stands for the amount of reacted organic gas. [c]ΔM mean particle mass concentration at steady state, which was obtained by multiplying SMPS-determined volume concentration by the assumed density of 1.0 g/cm^3 and was wall-loss corrected. [d]Relative humidity in the experiments was controlled by zero air and was lower than 2%.

In the context of NO_x and SO_2 copollution studies, the resulting SOA is characteristic of a high abundance of polar functional groups, which critically impact the formation mechanisms, yields, and physicochemical properties of SOA.[20,22,23,28]

β-Myrcene, one of the most common open-chain monoterpenes, exhibits high reactivity in the atmosphere.[29] Due to the ready influence of factors such as region and season, direct measurement of β-myrcene concentration is limited. In the field studies, the concentrations of β-myrcene in the Amazon rainforest were estimated to be in the range from a few to several hundred ppt.[30,31] Recent research studies indicated that β-myrcene not only significantly contributes to the recycling of OH radicals during oxidation processes but also exhibits the highest SOA yield among noncyclic terpenes, comparable to that of α-pinene.[32−34] While theoretical and laboratory studies have analyzed the ozonolysis and OH oxidation products (i.e., 4-vinyl-4-pentenal (4 V4P)) of β-myrcene, the understanding of the formation mechanism of high-mass products remains insufficient.[34,35] To address such a gap, this study utilized an online aerosol mass spectrometer to analyze chemical compositions of β-myrcene-derived SOA under various conditions, discovering a series of new compounds. Experimental results revealed remarkable differences in the roles of NO and NO_2 during β-myrcene photooxidation, as well as distinct synergistic effects between SO_2 and NO_x. Quantum chemical calculations were performed to elucidate the possible oxidation pathways.

2. MATERIALS AND METHODS

2.1. Smog Chamber Experimental System

β-Myrcene photooxidation experiments (Table 1) were studied in a 2 m^3 Teflon chamber, with a detailed description in the Supporting Information (SI). β-Myrcene (≥90.0%, Aladdin) and reaction gases were brought into the chamber by zero air. Only the molecular weight (MW) = 137 peak of β-myrcene was detected by the proton-transfer reaction mass spectrometer (PTR-QMS 3500, East & West Analytical Instruments, China), indicating the concentrations of impurities in the chamber were negligible. Initial concentrations of all reactants were recorded by gas analyzers (Models 42i, 43i, and 49i, Thermo Fisher Scientific, USA) following a 30 min equilibration period in the chamber. Particle size distribution, volume, and number concentrations were monitored by a scanning mobility particle sizer spectrometer (SMPS 3938L76, TSI Incorporated, USA).

Recently, laboratory studies at high concentrations of VOCs have contributed to understanding the complicated mechanisms of SOA formation, especially near the emission origins.[20,28,36,37] Notably, these formation mechanisms share fundamental common characteristics at an intrinsic level. In this study, considering that the vacuum ultraviolet free electron laser (VUV-FEL) beamline time is very expensive, the experiments were conducted at higher β-myrcene concentrations than those typically found in the atmosphere. Even though the concentrations listed in Table 1 do not reflect the actual atmospheric concentration of β-myrcene, the aim of this work was to provide insights into the mechanism of SOA formation in high-pollution areas.

2.2. Chemical Composition Characterization

The chemical compositions of SOA were detected by a VUV-FEL photoionization time-of-flight (TOF) aerosol mass spectrometer (abbreviated as VUV-FEL-TOF-AMS).[38] Threshold photoionization of the compounds is accessible by tuning the wavelength of the VUV-FEL (50−150 nm).[39] The mass resolution (M/ΔM) of VUV-FEL-TOF-AMS is about 4200 (Figure S1). Here, the mass spectral peak denotes the molecular ion and is written as the value of MW.

The oxidation states of SOA were analyzed by using the online electron ionization (EI) TOF-AMS (abbreviated as EI-TOF-AMS).[20,37,40] The known ion fragmentation of m/z = 44 (predominantly CO_2^+) and m/z = 43 (mainly $C_2H_3O^+$) enabled the extraction of the elemental ratio H:C and O:C.[41−44] EI-TOF-AMS organic signal

https://doi.org/10.1021/acs.est.5c10374
Environ. Sci. Technol. 2026, 60, 5097−5108

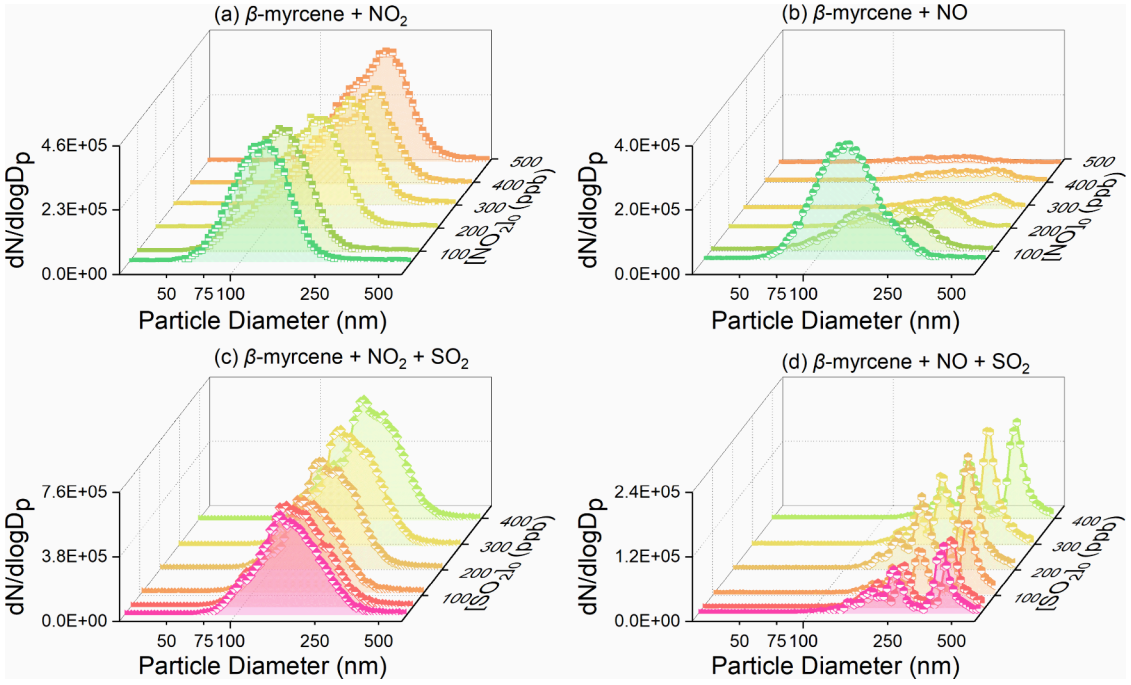

Figure 1. Particle number size distributions as a function of the $[NO_x]_0$ (a, b) and $[SO_2]_0$ (c, d) for all β-myrcene photooxidation experiments. D_p is the particle diameter. $dN/d\log D_p$ is the normalized number size distribution. The time point of PNSD was the second hour of the reaction, which was determined by the stabilization of the compositions of the SOA products via temporal evolution of particle size distribution of particles.

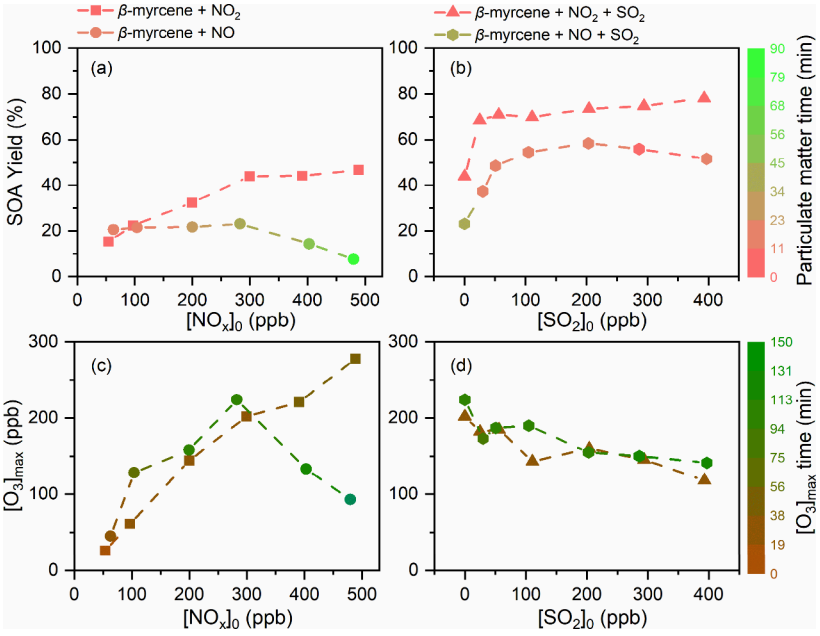

Figure 2. SOA yield and the generation time of particulate matter as a function of the $[NO_x]_0$ and $[SO_2]_0$ (a, b). The maximum ozone concentration and the occurrence time of $[O_3]_{max}$ as a function of $[NO_x]_0$ and $[SO_2]_0$ (c, d).

was normalized to nitrogen concentration to account for changes in the collection efficiency (see the SI for details).

2.3. Theoretical Methods

Quantum chemical calculations were performed by using the Gaussian 16 program package at the ωB97XD/aug-cc-pVTZ//M06−2X/def2-TZVP level of theory.[45] Relative energies included zero-point vibrational energy (ZPVE) corrections. The selection of present theoretical methods was based on recent studies on the effects of monoterpene photooxidation and ozonolysis.[46,47]

3. RESULTS AND DISCUSSION

3.1. Different Effects of $[NO_2]_0$ and $[NO]_0$ on β-Myrcene Photooxidation

As shown in Figure 1a, the mode diameter of particle number size distribution (PNSD) increases from 126.3 to 209.1 nm with the increase of $[NO_2]_0$ from 54 to 300 ppb and then converges with further increasing $[NO_2]_0$ up to 489 ppb. In contrast, the trend of the maximum particle number concentration exhibits only slight fluctuations (Figure S2). Differently, as $[NO]_0$ is

https://doi.org/10.1021/acs.est.5c10374
Environ. Sci. Technol. 2026, 60, 5097−5108

increased from 63 to 283 ppb, particle number concentrations exhibit a significant decline (Figure 1b), demonstrating that NO has a pronounced suppressive effect on NPF. The RO_2 + NO pathway was demonstrated to be a key oxidation pathway for VOCs.[14,48−51] In our experiments, high $[NO]_0$ enhances the reaction proportion of RO_2 and NO, leading to highly volatile organic nitrates, which could be the reason for the sharp decline in the particle number concentration. This will be confirmed by subsequent mass spectral analysis. Especially, with $[NO]_0$ increasing from 63 to 104 ppb, the PNSD shifts from unimodal to bimodal distribution and exhibits a broader range. Previous studies revealed significant differences in SOA formation mechanisms under different NO concentrations.[52,53] Thus, it is speculated that the variation of $[NO]_0$ may alter the branching ratio of RO_2 reactions with HO_2 and NO, thereby increasing the complexity of the photooxidation process. This may also explain the gradual increase in the mode diameter of PNSD within $[NO]_0$ = 63−283 ppb. As $[NO]_0$ increases from 283 to 480 ppb, highly volatile product formation becomes more favorable. Correspondingly, the increased consumption of NO subsequently inhibits its conversion to NO_2, leading to a reduced oxidant availability and a consequent decline in the mode diameter of PNSD.

Figure 2a shows how the SOA yields exhibit a different trend with increasing $[NO_x]_0$. In the NO_2 experiments, the trend of SOA yields parallels the evolution of the mode diameter of PNSD. In contrast, SOA yields remain stable within $[NO]_0$ = 63−283 ppb before declining significantly in the NO experiments. Significant differences appear in the timing trends of particulate matter generation between the two sets of experiments. In the NO_2 experiments, particulate matter formation begins within the first 10 min in all experiments. However, in the NO experiments, as $[NO]_0$ increases from 63 to 480 ppb, the generation time of particulate matter gradually increases from 16 to 81 min. Such distinctions suggest that while there is mutual conversion between NO_2 and NO during the NO_x cycle, the initial component of photooxidation experiments has a crucial impact on VOCs oxidation. As a critical component within the NO_x cycle, NO_2 serves as the initiating step, playing a critical role in oxidant formation and facilitating subsequent oxidation processes.[48] In the NO_2 experiments, the abundant NO_2 serves as a rich source of oxidants, facilitating β-myrcene oxidation and thereby promoting the SOA yield. In the NO experiments, a large amount of NO significantly affects the fate of RO_2, thereby suppressing the SOA yield. Furthermore, NO undergoes a conversion process to NO_2 to initiate oxidant formation in the NO_x cycle. High $[NO]_0$ prolongs the conversion period, delaying oxidant formation and ultimately shifting the timing of particulate matter generation to later stages.

In the NO_x cycle, O_3 is primarily generated through the NO_2 photolysis.[49] Under fixed $[BVOC]_0$, the occurrence time of $[O_3]_{max}$ is correlated with the timing of particle formation.[18,20,24] Therefore, $[O_3]_{max}$ and its occurrence time can serve as indicators of the photooxidation process. As shown in Figure 2c, a comparison of $[O_3]_{max}$ reveals distinctly different trends in the NO_x experiments. In the NO_2 experiments, as $[NO_2]_0$ increases from 54 to 489 ppb, $[O_3]_{max}$ rises continuously from 26 to 278 ppb, while the occurrence time of $[O_3]_{max}$ remains relatively stable. This indicates that as $[O_3]_{max}$ produced from the photolysis of NO_2 increases, the ozonolysis may become increasingly significant. In contrast, in the NO experiments, $[O_3]_{max}$ exhibits a nonlinear response, consistent with previous smog chamber studies.[18,20,37] This could be attributed to the fact that as $[NO]_0$ rises to 283 ppb, more NO significantly alters the fate of RO_2, favoring $RONO_2$ formation. The consumption of RO_2 not only disrupts the RO_x cycle but also perturbs the dynamic balance of NO_x: acting as a sink for NO_x, the generation of $RONO_2$ reduces the interconversion between NO and NO_2, suppressing the key process of ozone production initiated by NO_2 photolysis and ultimately inhibiting the O_3 formation.

Notable discrepancies in SOA formation primarily stemmed from the NO_x cycle. NO_2 rapidly provides oxidants, facilitating VOC oxidation. Once the vapor of oxidation products becomes supersaturated, they are transformed into particle form, and a large amount of particulate matter will be produced in a short period of time. Though NO_2 can affect RO_2 chemistry, its products are thermodynamically unstable during the photooxidation process, indicative of insignificant impact.[48] In the NO experiments, NO can directly participate in oxidation reactions, increasing the volatility of the products and thereby inhibiting particle formation. Additionally, NO must first be converted to NO_2 to drive oxidant formation. While the delayed effect of this process may suppress particle formation, the extended reaction time provides for oxidation processes, which, in turn, promote subsequent particle size growth.

3.2. Synergistic Effects of $[SO_2]_0$ and $[NO_x]_0$ on SOA Formation

As demonstrated in Figure 1c and d, the change of $[SO_2]_0$ mainly impacts the particle number concentrations for the oxidation products. With SO_2 added, the particle number concentration increases significantly in NO_x experiments (Figure S3). This is likely due to the fact that SO_2 is oxidized by OH or stabilized Criegee intermediates (sCIs) to form H_2SO_4. On one hand, the generated H_2SO_4 serves as acid seeds, facilitating the condensation of oxidation products in the gas phase by increasing the available surface area and volume. On the other hand, H_2SO_4 enhances the heterogeneous reactions under appropriate humidity, leading to the formation of organosulfates and promoting the generation of new particles. It has been found that the acid-catalyzed reactions at RH of ∼25 and ∼50% could be effective for some monoterpenes and anthropogenic VOCs.[28,54]

Compared to the SO_2-free experiments, the SOA yields show an increasing trend in SO_2 experiments (Figure 2b). The difference is that adding more than 25 ppb of SO_2 in the NO_2 experiments, SOA yields basically tend to converge; in the NO experiments, as $[SO_2]_0$ ranged from 30 to 203 ppb, SOA yields increase slightly and then tend to converge. We consider that H_2SO_4 may be a main contributor to the observed increase in particle number concentration, which subsequently enhances the SOA yields. More importantly, the addition of SO_2 does not significantly affect the generation time of particulate matter in the NO_2 experiments; but in the NO experiments, generation time gradually decreases from 38 to 11 min. According to the dominating role of H_2SO_4 in nucleation investigated by binary, ternary, and ion-induced nucleation theories,[25,55] the generation of OH during the conversion of NO to NO_2 facilitates the formation of H_2SO_4, leading to an earlier onset of particulate matter in the NO experiments. In addition, $[O_3]_{max}$ decreases with the increase of $[SO_2]_0$ in NO_x experiments, suggesting that the ozonolysis plays a more significant role in the presence of SO_2. Besides, the occurrence time of $[O_3]_{max}$ remains constant despite increasing $[SO_2]_0$, suggesting that SO_2 does not interfere with the NO_x cycle.

https://doi.org/10.1021/acs.est.5c10374
Environ. Sci. Technol. 2026, 60, 5097−5108

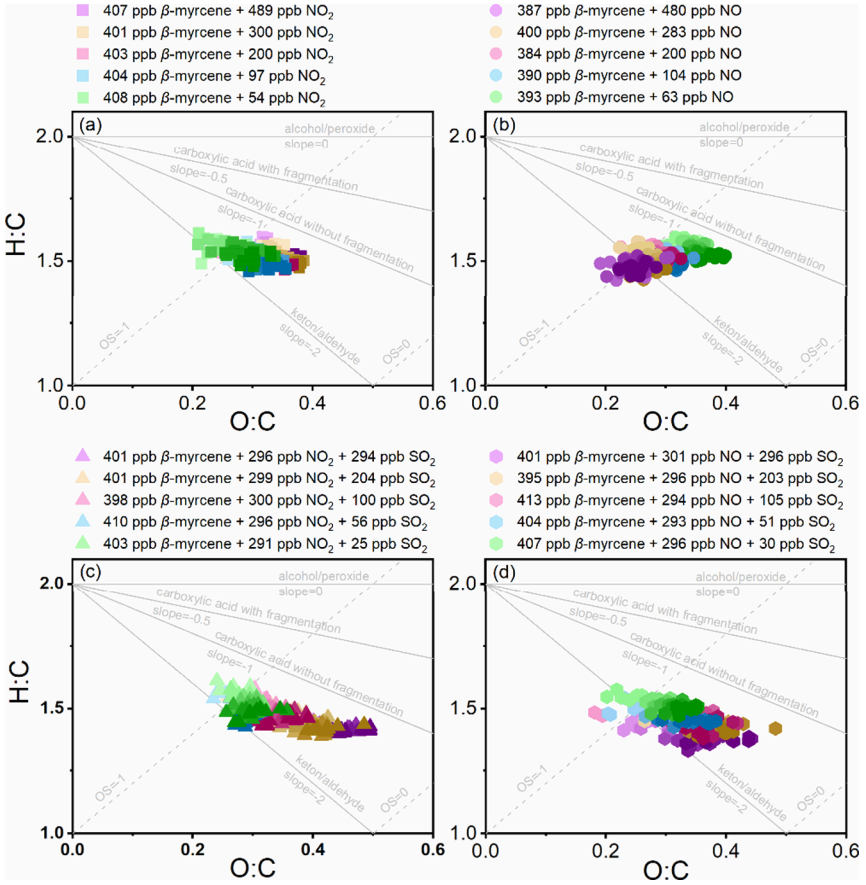

Figure 3. Van Krevelen diagram for β-myrcene photooxidation experiments. The gradual darkening of icon color denotes time evolution, which data points were collected every 5 min over a total period of 5 h. Specifically, slope = 0 means the replacement of a hydrogen atom (−H) on an aliphatic carbon (−CH_2−) by an alcohol group (−OH) or a peroxide group (−OOH); the slope of −1/0.5 corresponds to the formation of a carboxylic acid group (−C(=O)OH); and the slope of −2 represents a ketone or aldehyde group (−C(=O)−) replaces an −CH_2−.

3.3. Molecular Characteristics of SOA

In the V−K diagram (Figure 3), the dotted line represents the oxidation state (OS), which is an important parameter for describing the oxidative evolution of organic aerosols and assessing their atmospheric aging state.[56] During all photooxidation experiments, the OSs' values of oxidation products exhibited a consistent increase from −1 to 0 over time, indicating a systematic increase in both the abundance of oxygen-containing functional groups and the average oxidation state of the products. Different functionalization reactions alter the elemental ratios of O:C and H:C. The black straight lines represent the addition of specific functional groups to aliphatic carbons that are initially unfunctionalized.[57,58]

In Figure 3a, the O:C ratio increases significantly as $[NO_2]_0$ increases from 54 to 300 ppb, suggesting that oxygen-containing functional groups are effectively incorporated into the product. In contrast, the O:C ratio exhibits a marked decrease with increasing $[NO]_0$ (Figure 3b), indicating that higher $[NO]_0$ inhibits the increase of OSs. Previous studies have shown that $RONO_2$ generally had relatively high vapor pressures, and their formation could significantly reduce the OSs of the products.[48,50,51,59] The result in Figure 3b shows that the reaction pathway (RO_2 + NO → $RONO_2$) likely becomes increasingly significant as $[NO]_0$ increases in the NO experiments, corroborating our aforementioned speculation. The values of slope in the NO_2 experiments are found to fall within the range of −1 to −0.5, whereas those in the NO experiments are greater than −0.5. This suggests that in the NO_2 experiments, the oxidation products tend to form carboxylic acids or lipid peroxide, while in the NO experiments, the oxidation products predominantly contain alcohol and peroxide groups. The oxidation effect in the NO_2 experiments is significantly stronger than that in the NO experiments.

As shown in Figure 3c,d, an increase in $[SO_2]_0$ leads to a significant rise in the O:C ratio in NO_x experiments, accompanied by a notable decrease in the H:C ratio. The reduction in H:C is typically associated with processes such as hydrogen abstraction, dehydration, and oxidation. It is speculated that the reactions such as ROH + H_2SO_4 → $ROSO_3H$ + H_2O may occur in these experiments. Such formation of organosulfates has been previously observed in other monoterpene oxidation studies.[22,23] These organosulfates likely exhibit a sulfate ester structure, which significantly enhances the oxidation state of the product.

Furthermore, the increase in the O:C ratio in the NO_2 experiments is more pronounced than that in the NO experiments. This difference may be attributed to the abundance of oxidants in the NO_2 experiments, which could enhance the formation of more sulfate particles. These particles serve as sites for multiphase reactions and facilitate the capture of low oxidation products from the gas phase into the particle phase, thereby increasing the overall OSs of SOA. In the NO experiments, the presence of organic nitrates may influence the increase in the O:C ratio, which may explain why the O:C

https://doi.org/10.1021/acs.est.5c10374
Environ. Sci. Technol. 2026, 60, 5097−5108

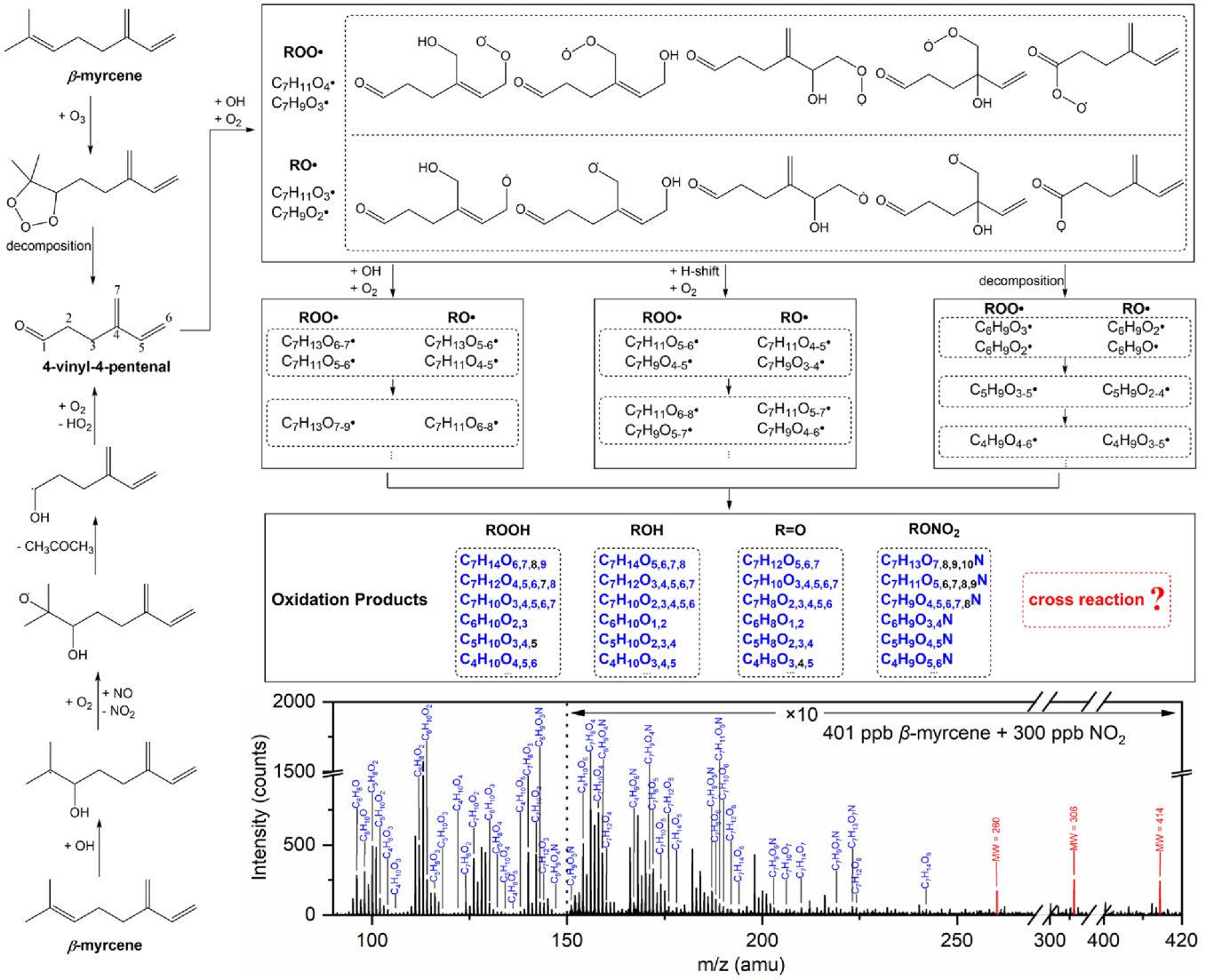

Figure 4. Summary of potential formation mechanisms of oxidation compounds generated by β-myrcene photooxidation. The possibility of other oxidation pathways and products is not excluded.

ratio increased more slowly. Oxidation products containing multifunctional groups ($-ONO_2$ and $-OSO_3H$) have been recently identified in the monoterpene oxidation[22,23,28] and are also likely formed in this work.

3.4. Molecular Composition of β-Myrcene Photooxidation

The studies on β-myrcene oxidation revealed the preferential reactivity of independent double bonds with oxidants and identified the 4 V4P as a key SOA precursor.[34,35,34,35,60−63] In this work, O_3 is produced via the NO_x cycle and is likely the principal and initial oxidant responsible for triggering β-myrcene oxidation. Recent investigations have underscored the pivotal role of O_3 in photooxidation processes.[19,24] Specifically, β-myrcene reacts with O_3 to yield primary ozonide (POZ), which is very unstable and rapidly decomposes to produce sCIs, contributing further to aerosol formation.[35] Previous studies have consistently identified a series of gas-phase products (MW = 58, 110, 112, 114, and 138) during the β-myrcene oxidation.[34,62−64] Since acetone was identified as one of the key products, it was detected by using the PTR-QMS in this work (Figure S4). The MW signals of 110, 112, 114, and 138 were also successfully detected in the VUV-FEL-TOF-AMS mass spectra (Figure 4). It is suggested that these compounds may partition into the particle phase or undergo continuous oxidation due to double bonds in their molecular structures, leading to their absence in the gas-phase measurements.

Figure 4 shows a summary of the β-myrcene oxidation mechanism, indicating that most oxidation products match well in the mass spectrum. The partial deviation of mass spectra of $RONO_2$ could be rationalized by the fact that RO_2 may be consumed by other competing reaction pathways, reducing its reaction with NO. While under relatively high NO_x conditions, the rate constants for RO_2 autoxidation and self-/cross-reactions in monoterpene oxidation were found to be sufficiently fast to compete effectively with the RO_2 + NO pathway.[10,65] The branching ratio for $RONO_2$ from β-myrcene oxidation constituted only approximately 13% of the total RO_2 + NO reactions, underscoring a preference for the formation of other oxidation products over $RONO_2$.[34] Moreover, the introduction of nitrogen-containing groups elevated the saturation vapor pressure of these compounds.[51] Even for some $RONO_2$ molecules (with carbon numbers up to $\sim C_{12}$), the vapor pressure remained too high to favor partitioning to the particle phase,[50] which might be a reason for the absence of a part of

https://doi.org/10.1021/acs.est.5c10374
Environ. Sci. Technol. 2026, 60, 5097−5108

larger $RONO_2$ in the mass spectra. Notably, several peaks with high intensities and irregular changes (MW = 260, 306, and 414) are also observed, which may originate from cross-reactions.

In the previous VUV-FEL-TOF-AMS studies of monoterpenes photooxidation, comparative analysis of mass spectra at different wavelengths revealed that the 125.0 nm wavelength was suitable for the detection of oxidation products (i.e., organic peroxides, organic nitrates, and esters).[18,20] The VUV-FEL-TOF-AMS experiments on the Δ^3-carene + NO_2 + SO_2 system at the 125, 115, and 105 nm wavelengths indicated that the wavelength of 115.0 nm was optimal for threshold photoionization of most organosulfates.[20] Considering that the scan of VUV-FEL wavelength is not as readily available as synchrotron radiation light source and the ionization thresholds of the homologues generated from β-myrcene photooxidation could be similar to those from the α-pinene and Δ^3-carene systems, we measured the mass spectra at the VUV-FEL wavelengths of 115 and 125 nm in this work. Recently, photoionization efficiency spectroscopic studies on Δ^3-carene oxidation identified the compounds with MW $\leq$ 200.[66,67] In this work, we mainly focus on the analysis of mass spectra in the range of MW > 200 with fewer fragments, for which the mass resolution is reliable to identify the compounds.

Optimizing VUV-FEL wavelength and pulse energy could achieve high sensitivity and selectivity in threshold photoionization for monoterpene oxidation experiments.[18,20,24,47] Mass spectra of SOA generated by β-myrcene + NO_x and β-myrcene + NO_x + SO_2 were measured at the VUV-FEL wavelengths of 125 and 115 nm, respectively. In Figure 5a,b, the MW = 168, 184, and 216 peaks are observed, which are consistent with the confirmed products of β-myrcene oxidation as reported in literature.[33,36,63,68] This consistency demonstrates the reliability of the VUV-FEL-TOF-AMS.

In Figure 5a, new peaks are observed at MW = 260, 306, and 414, respectively, which are hypothesized to be the accretion products of ROOR′. In contrast with Figure 5a, the MW = 306 peak disappears in Figure 5b, whereas the intensities of the MW = 260 and 414 peaks are obviously reduced but still observable; a new peak appears at MW = 223 and is tentatively identified as an organic nitrate. The overall number and intensities of mass spectral peaks of SOA in the NO_2 experiment are significantly higher than those in the NO experiment (Table S1). This indicates that the generation of particulate matter is more favorable in the NO_2 experiment, and its chemical composition is more complex. The mass spectra of Figure 5c,d reveal the newly observed peaks at MW = 212, 240, 287, and 304, respectively. Indeed, the intensity of the 414 peak (organic peroxide) measured at the high VUV energy of 115 nm/10.8 eV (Figure 5c) is obviously reduced as compared to that at the low VUV energy of 125 nm/9.9 eV (Figure 5a), indicating that the photoionization at 125 nm is more suitable for detection of organic peroxides, whereas the photoionization at 115 nm is favorable for detection of organosulfates. Therefore, the newly observed peaks at 115 nm provide evidence for the formation of organosulfates that are promoted by the addition of SO_2. Notably, a new peak at MW = 287 (Figure 5d) is hypothesized to be an oxidation product containing both -ONO_2 and -OSO_3H functional groups. Compared with Figure 5c, the overall peak intensities in Figure 5d decrease, and the MW = 304 peak disappears. This reduction may be attributed to the process of NPF inhibitory effects in the NO experiments.

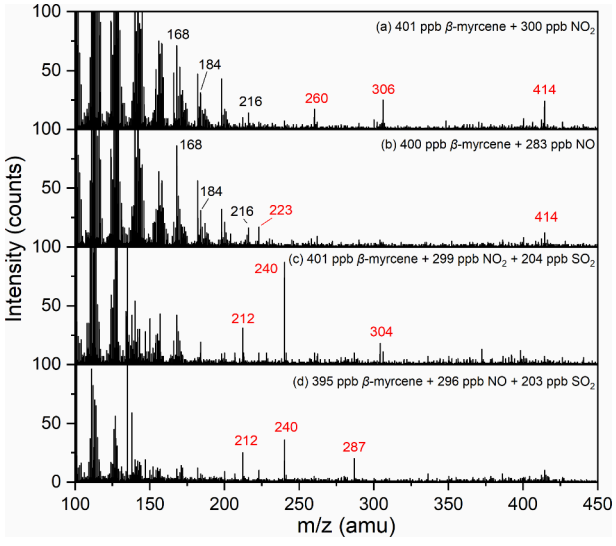

Figure 5. VUV-FEL photoionization mass spectra of the compounds generated under different experimental conditions. The compounds were ionized by the VUV-FEL at 125.0 (a, b) and 115.0 nm (c, d). New compounds are marked with red, and the background of all mass spectra has been subtracted. The time point of mass spectra was the third hour of the reaction, which was determined by the stabilization of the compositions of the SOA products via temporal evolution of particle mass concentrations (Figure S5).

β-Myrcene ozonolysis experiments were performed to further confirm the generation pathway of oxidation products (Table S2 and Figures S6 and S7). The MW = 260, 306, and 414 peaks are observed in the ozonolysis experiments (Figure S8a), suggesting that most oxidation products originate from the OH or O_3 oxidation pathway. After introducing the OH scavenger (cyclohexane) (Figure S8b), all the peaks are still observable but exhibit varying degrees of intensity reduction. This demonstrates that these cross-products are formed simultaneously in both the OH and the O_3 oxidation pathways and are likely the oxidation products of 4 V4P. The presence of the MW = 212 and 304 peaks in both experiments (Figure S8c,d) indicates that these peaks might be organosulfates formed through the oxidation of 4 V4P. After adding cyclohexane (Figure S8d), the MW = 240 peak disappears, indicative of its formation from the OH oxidation. Notably, the MW = 223 and 287 peaks are absent in the ozonolysis experiments, suggesting that these compounds contain nitro groups.

3.5. Possible Formation Mechanisms of New Compounds

Based on quantum chemical calculations, formation pathways for the newly observed compounds were proposed and were predicted to be thermodynamically favorable and kinetically feasible. For most pathways, the corresponding rate constants have been previously reported (Table S3).[34,35,49,65,34,35,69−71] Molecular formulas of the compounds are given in Table S4. We do not exclude alternative structures/pathways.

As shown in Figure 6, the reaction between β-myrcene and OH initiates free radical propagation, leading to the formation of multiple intermediates ($\mathbf{M_{OH}}$-**I***y* (*y* = 1−4)). Then, NO terminates the oxidation reaction of $\mathbf{M_{OH}}$-**I4**, forming $\mathbf{M_{OH}}$-**P3** (MW = 223). Conjugated double bond addition is calculated to be most favorable at the terminal carbon of the branch chain (Table S5), forming $\mathbf{M_{OH}}$-**P1** and $\mathbf{M_{OH}}$-**P2**. The ROH structural products from monoterpene oxidation undergo nucleophilic substitution reactions involving H_2SO_4.[72] $\mathbf{M_{OH}}$-**P4** is proposed

https://doi.org/10.1021/acs.est.5c10374
Environ. Sci. Technol. 2026, 60, 5097−5108

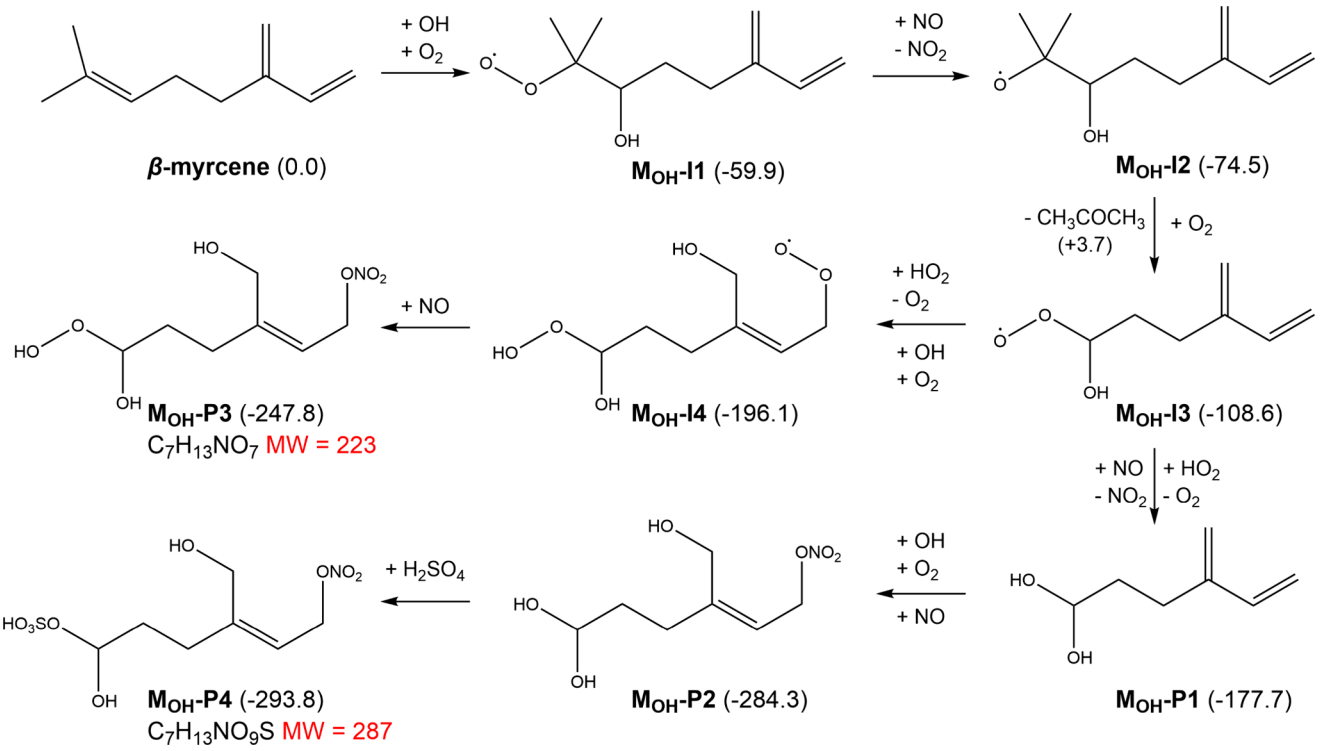

Figure 6. Possible formation mechanisms of new compounds MW = 223 and 287 calculated at the ωB97XD/aug-cc-pVTZ//M06−2X/def2-TZVP level of theory. Relative energies are given in kcal/mol. The new compounds are labeled as $\mathbf{M_{OH}}$-**P***x* (x = 1−4) sorted by molecular weight, and the intermediates are successively labeled as $\mathbf{M_{OH}}$-**I***y* (y = 1−4).

to be the condensation product generated through the synergistic interaction of SO_2 and NO.

Based on the analysis of Section 3.4, we suppose that the MW = 260, 306, and 414 compounds resulted from 4 V4P oxidation (Figures S9 and S10). The H-abstraction is a pivotal mechanism during monoterpene oxidation.[73] Consequently, the formation mechanisms of these three compounds could be initiated from the H-abstraction reaction (Figure S10). The formation of **M-I***y* (y = 1−7) primarily encompasses OH-addition, decomposition, and bimolecular reaction. Several studies indicated that RO_2 cross-reaction is one of the important pathways for monoterpenes oxidation.[74,75] **M-I4** and **M-I7** undergo cross-reactions with **M-I9** (Figure S11), forming **M-P1** (MW = 260) and **M-P3** (MW = 414). Similar mechanisms yielded **M-P2** (MW = 304). **M-P***x* (x = 1−3) possess multifunctional groups (ester, acid, alcohol, etc.), which significantly enlarge the O:C ratio of the compounds.

Figure S12 shows the possible formation processes of the MW = 212, 240, and 304 compounds, which are primarily initiated from **M-I7**/**M-I8** and $\mathbf{M_{OH}}$-**P1**. We hypothesize that **M-OS-P***x* (x = 1−3) (MW = 212, 240, and 304) are organosulfates, potentially formed by esterification of oxidation products with H_2SO_4. These multiphase reactions represent a significant SO_2-enhancement mechanism for SOA formation, converting higher-volatility oxygenates into lower-volatility organosulfates incorporated into the particle phase. Indeed, recent studies indicated that the reaction of SO_2 with organic peroxides formed through monoterpene oxidation could effectively facilitate organosulfate formation.[54,76]

Previous studies indicated that under dry conditions, sulfuric acid could be formed from the reactions of sCIs with SO_2 and enhanced SOA formation through the acid-catalyzed mechanisms.[54,77] Nevertheless, the heterogeneous acid-catalyzed reaction may not be the key contributor to the SOA formation under our experimental conditions with RH close to zero. This work suggests that the gas-phase formation pathways also contribute appreciably to organosulate mass in SOA. Field observations revealed that some organosulfates remained stable in both gas and particle phases.[78,79] Laboratory studies on the monoterpene oxidation also indicated that organosulfates might originate from the reaction of SO_3 with oxidized organic molecules.[80] Recent observation of gas-phase glycolic acid sulfate verified the contribution of gas-phase reactions to organosulfate formation.[81]

4. ENVIRONMENTAL IMPLICATIONS

This study systematically investigated SOA formation from β-myrcene photooxidation with NO_x and SO_2. With the unique capabilities of VUV-FEL-TOF-AMS, we discovered a series of new compounds. A key finding is the significant difference in the roles of NO_2 and NO during the photooxidation process. NO_2 not only promotes particle formation but also enhances the generation of oxygenated organic compounds. However, NO_2 induces abundant oxidants, leading to the formation of smaller particles. In contrast, NO initially suppresses particle formation but promotes particle size growth in later stages through a "delayed effect". NO directly participates in oxidation reactions, reducing the oxidative states of the products. While highly oxygenated organic compounds (MW = 260, 306, and 414) are detected in the NO_2 experiments, the overall mass spectral intensities of compounds are reduced in the NO experiments, with a characteristic peak concentrated in compound (MW = 223) containing nitrogen−oxygen functional groups.

The coexistence of SO_2 and NO_x significantly enhances SOA yields, which could be due to the partial contribution from the organosulfate formation. We identified new compounds with

https://doi.org/10.1021/acs.est.5c10374
Environ. Sci. Technol. 2026, 60, 5097−5108

MW values of 212, 240, 287, and 304 in the β-myrcene + SO_2 + NO_x experiments. The MW = 287 compound was characterized as a multifunctional oxidized complex containing both $-OSO_3H$ and $-ONO_2$ groups. The identification and analysis of these novel compounds help to correct the biases in SOA formation predictions, providing more precise data for understanding aerosol formation mechanisms in regions influenced by both anthropogenic and biogenic sources.

■ ASSOCIATED CONTENT

Supporting Information

The Supporting Information is available free of charge at https://pubs.acs.org/doi/10.1021/acs.est.5c10374.

Experimental details; detailed information of VUV-FEL-TOF-AMS (Figure S1); temporal evolution of particle size distribution in the photooxidation experiments (Figures S2 and S3); temporal evolution of [acetone] (Figure S4); particle mass concentrations in the photooxidation experiments (Figures S5); temporal evolution of particle size distribution and particle mass concentrations in the ozonolysis experiments (Figures S6 and S7); comparison of mass spectra at different $\lambda_{VUV\text{-}FEL}$ (Figure S8); detailed mechanisms of the β-myrcene photooxidation (Figures S9−S12); positions and intensities of mass peaks shown in Figure 5 (Table S1); initial conditions and results for the β-myrcene ozonolysis experiments (Table S2); general rate constants for relevant pathways (Table S3); new compounds identified in the photooxidation of β-myrcene (Table S4); different structures of radical MW = 127 (Table S5) (PDF)

■ AUTHOR INFORMATION

Corresponding Authors

Gang Li − *State Key Laboratory of Chemical Reaction Dynamics and Dalian Coherent Light Source, Dalian Institute of Chemical Physics, Chinese Academy of Sciences, Dalian 116023, China; University of Chinese Academy of Sciences, Beijing 100049, China;* orcid.org/0000-0001-5984-111X; Email: gli@dicp.ac.cn

Ling Jiang − *State Key Laboratory of Chemical Reaction Dynamics and Dalian Coherent Light Source, Dalian Institute of Chemical Physics, Chinese Academy of Sciences, Dalian 116023, China; University of Chinese Academy of Sciences, Beijing 100049, China; Hefei National Laboratory, Hefei 230088, China;* orcid.org/0000-0002-8485-8893; Phone: +86-411-84379857; Email: ljiang@dicp.ac.cn

Authors

Ya Zhao − *School of Chemistry, Dalian University of Technology, Dalian 116024, China; State Key Laboratory of Chemical Reaction Dynamics and Dalian Coherent Light Source, Dalian Institute of Chemical Physics, Chinese Academy of Sciences, Dalian 116023, China; University of Chinese Academy of Sciences, Beijing 100049, China*

Chong Wang − *Institute of Advanced Light Source Facilities, Shenzhen 518107, China; Department of Chemical Physics, University of Science and Technology of China, Hefei 230026, China*

Yingqi Zhao − *State Key Laboratory of Chemical Reaction Dynamics and Dalian Coherent Light Source, Dalian Institute of Chemical Physics, Chinese Academy of Sciences, Dalian 116023, China; University of Chinese Academy of Sciences, Beijing 100049, China*

Yufeng Shao − *State Key Laboratory of Chemical Reaction Dynamics and Dalian Coherent Light Source, Dalian Institute of Chemical Physics, Chinese Academy of Sciences, Dalian 116023, China; University of Chinese Academy of Sciences, Beijing 100049, China*

Hua Xie − *State Key Laboratory of Chemical Reaction Dynamics and Dalian Coherent Light Source, Dalian Institute of Chemical Physics, Chinese Academy of Sciences, Dalian 116023, China; University of Chinese Academy of Sciences, Beijing 100049, China;* orcid.org/0000-0003-2091-6457

Jiayue Yang − *State Key Laboratory of Chemical Reaction Dynamics and Dalian Coherent Light Source, Dalian Institute of Chemical Physics, Chinese Academy of Sciences, Dalian 116023, China; University of Chinese Academy of Sciences, Beijing 100049, China*

Weiqing Zhang − *State Key Laboratory of Chemical Reaction Dynamics and Dalian Coherent Light Source, Dalian Institute of Chemical Physics, Chinese Academy of Sciences, Dalian 116023, China; University of Chinese Academy of Sciences, Beijing 100049, China;* orcid.org/0000-0001-6518-4152

Guorong Wu − *State Key Laboratory of Chemical Reaction Dynamics and Dalian Coherent Light Source, Dalian Institute of Chemical Physics, Chinese Academy of Sciences, Dalian 116023, China; University of Chinese Academy of Sciences, Beijing 100049, China;* orcid.org/0000-0002-0212-183X

Xueming Yang − *School of Chemistry, Dalian University of Technology, Dalian 116024, China; State Key Laboratory of Chemical Reaction Dynamics and Dalian Coherent Light Source, Dalian Institute of Chemical Physics, Chinese Academy of Sciences, Dalian 116023, China; University of Chinese Academy of Sciences, Beijing 100049, China; Institute of Advanced Light Source Facilities, Shenzhen 518107, China; Hefei National Laboratory, Hefei 230088, China; Department of Chemistry and Guangdong Provincial Key Laboratory of Catalytic Chemistry, Southern University of Science and Technology, Shenzhen 518055, China;* orcid.org/0000-0001-6684-9187

Complete contact information is available at: https://pubs.acs.org/10.1021/acs.est.5c10374

Notes

The authors declare no competing financial interest.

■ ACKNOWLEDGMENTS

The authors gratefully acknowledge the staff members of the Dalian Coherent Light Source (31127.02.DCLS) for technical support and assistance in data collection. This work was supported by the National Natural Science Foundation of China (nos. 22125303, 92361302, 22103082, 22273101, 22288201, and 21327901), the Strategic Priority Research Program of the Chinese Academy of Sciences (XDB0970100), the National Key Research and Development Program of China (no. 2021YFA1400501), the Innovation Program for Quantum Science and Technology (no. 2021ZD0303304), Dalian Institute of Chemical Physics (DICP I202437), Chinese Academy of Sciences (no. GJJSTD20220001), and the International Partnership Program of the Chinese Academy of Sciences (121421KYSB20170012).

REFERENCES

(1) An, Z. S.; Huang, R. J.; Zhang, R. Y.; Tie, X. X.; Li, G. H.; Cao, J. J.; Zhou, W. J.; Shi, Z. G.; Han, Y. M.; Gu, Z. L.; Ji, Y. M. Severe haze in northern China: A synergy of anthropogenic emissions and atmospheric processes. *Proc. Natl. Acad. Sci. U.S.A.* **2019**, *116*, 8657−8666.

(2) Cui, L. L.; Wu, D.; Wang, S. X.; Xu, Q. C.; Hu, R. L.; Hao, J. M. Measurement report: Ambient volatile organic compound (VOC) pollution in urban Beijing: Characteristics, sources, and implications for pollution control. *Atmos. Chem. Phys.* **2022**, *22*, 11931−11944.

(3) Zheng, Y.; Chen, Q.; Cheng, X.; Mohr, C.; Cai, J.; Huang, W.; Shrivastava, M.; Ye, P. L.; Fu, P. Q.; Shi, X. D.; Ge, Y. L.; Liao, K. R.; Miao, R. Q.; Qiu, X. H.; Koenig, T. K.; Chen, S. Y. Precursors and pathways leading to enhanced secondary organic aerosol formation during severe haze episodes. *Environ. Sci. Technol.* **2021**, *55*, 15680−15693.

(4) Hui, L.; Liu, X.; Tan, Q.; Feng, M.; An, J.; Qu, Y.; Zhang, Y.; Cheng, N. VOC characteristics, sources and contributions to SOA formation during haze events in Wuhan, central China. *Sci. Total Environ.* **2019**, *650*, 2624−2639.

(5) Yu, S. J.; Xue, C. F.; Deng, F. W.; Xu, Q. X.; Zhao, B. N. VOCs concentration, SOA formation contribution and festival effects during heavy haze event: A case study in Zhengzhou, central China. *Atmosphere* **2024**, *15*, 1009.

(6) Qiang, Y.; Cao, Q.; Xia, L. J.; Chen, Y. Q.; Wu, X. Y.; Chi, H. China's antismog push faces challenges. *Science* **2025**, *389*, 135.

(7) Liang, C. W.; Chang, C. C.; Liang, J. J. The impacts of air quality and secondary organic aerosols formation on traffic accidents in heavy fog-haze weather. *Heliyon* **2023**, *9*, No. e14631.

(8) Fan, L. H.; Yan, X. J.; Du, Q. Y.; Zhang, J. X.; Liu, G. H.; Yang, Y. X.; Miao, Y. R.; Zhang, G. Q. On the sources of ambient SOA in $PM_{2.5}$: An integrated analysis over Jinan city of China. *Atmos. Pollut. Res.* **2024**, *15*, No. 102008.

(9) Chu, B.; Chen, T.; Liu, Y.; Ma, Q.; Mu, Y.; Wang, Y.; Ma, J.; Zhang, P.; Liu, J.; Liu, C.; Gui, H.; Hu, R.; Hu, B.; Wang, X.; Wang, Y.; Liu, J.; Xie, P.; Chen, J.; Liu, Q.; Jiang, J.; Li, J.; He, K.; Liu, W.; Jiang, G.; Hao, J.; He, H. Application of smog chambers in atmospheric process studies. *Natl. Sci. Rev.* **2022**, *9*, No. nwab103.

(10) Wang, S. Y.; Zhao, Y.; Chan, A. W. H.; Yao, M.; Chen, Z. M.; Abbatt, J. P. D. Organic peroxides in aerosol: Key reactive intermediates for multiphase processes in the atmosphere. *Chem. Rev.* **2023**, *123*, 1635−1679.

(11) Sarrafzadeh, M.; Wildt, J.; Pullinen, I.; Springer, M.; Kleist, E.; Tillmann, R.; Schmitt, S. H.; Wu, C.; Mentel, T. F.; Zhao, D.; Hastie, D. R.; Kiendler-Scharr, A. Impact of NO_x and OH on secondary organic aerosol formation from β-pinene photooxidation. *Atmos. Chem. Phys.* **2016**, *16*, 11237−11248.

(12) Draper, D.; Farmer, D.; Desyaterik, Y.; Fry, J. A qualitative comparison of secondary organic aerosol yields and composition from ozonolysis of monoterpenes at varying concentrations of NO_2. *Atmos. Chem. Phys.* **2015**, *15*, 12267−12281.

(13) Pye, H. O. T.; D'Ambro, E. L.; Lee, B. H.; Schobesberger, S.; Takeuchi, M.; Zhao, Y.; Lopez-Hilfiker, F.; Liu, J.; Shilling, J. E.; Xing, J.; Mathur, R.; Middlebrook, A. M.; Liao, J.; Welti, A.; Graus, M.; Warneke, C.; de Gouw, J. A.; Holloway, J. S.; Ryerson, T. B.; Pollack, I. B.; Thornton, J. A. Anthropogenic enhancements to production of highly oxygenated molecules from autoxidation. *Proc. Natl. Acad. Sci. U.S.A.* **2019**, *116*, 6641−6646.

(14) Nie, W.; Yan, C.; Yang, L.; Roldin, P.; Liu, Y.; Vogel, A. L.; Molteni, U.; Stolzenburg, D.; Finkenzeller, H.; Amorim, A.; Bianchi, F.; Curtius, J.; Dada, L.; Draper, D. C.; Duplissy, J.; Hansel, A.; He, X. C.; Hofbauer, V.; Jokinen, T.; Kim, C.; Lehtipalo, K.; Nichman, L.; Mauldin, R. L.; Makhmutov, V.; Mentler, B.; Mizelli-Ojdanic, A.; Petäjä, T.; Quéléver, L. L. J.; Schallhart, S.; Simon, M.; Tauber, C.; Tomé, A.; Volkamer, R.; Wagner, A. C.; Wagner, R.; Wang, M.; Ye, P.; Li, H.; Huang, W.; Qi, X.; Lou, S.; Liu, T.; Chi, X.; Dommen, J.; Baltensperger, U.; El Haddad, I.; Kirkby, J.; Worsnop, D.; Kulmala, M.; Donahue, N. M.; Ehn, M.; Ding, A. NO at low concentration can enhance the formation of highly oxygenated biogenic molecules in the atmosphere. *Nat. Commun.* **2023**, *14*, 3347.

(15) Schervish, M.; Donahue, N. M. Peroxy radical chemistry and the volatility basis set. *Atmos. Chem. Phys.* **2020**, *20*, 1183−1199.

(16) Zhao, D. F.; Schmitt, S. H.; Wang, M. J.; Acir, I. H.; Tillmann, R.; Tan, Z. F.; Novelli, A.; Fuchs, H.; Pullinen, I.; Wegener, R.; Rohrer, F.; Wildt, J.; Kiendler-Scharr, A.; Wahner, A.; Mentel, T. F. Effects of NO_x and SO_2 on the secondary organic aerosol formation from photooxidation of α-pinene and limonene. *Atmos. Chem. Phys.* **2018**, *18*, 1611−1628.

(17) Aruffo, E.; Wang, J.; Ye, J.; Ohno, P.; Qin, Y.; Stewart, M.; McKinney, K.; Di Carlo, P.; Martin, S. T. Partitioning of organonitrates in the production of secondary organic aerosols from α-pinene photooxidation. *Environ. Sci. Technol.* **2022**, *56*, 5421−5429.

(18) Zhao, Y.; Zhang, Z.; Zhao, Y.; Wang, C.; Xie, H.; Yang, J.; Zhang, W.; Wu, G.; Li, G.; Jiang, L.; Yang, X. Effects of NO_x and NH_3 on the secondary organic aerosol formation from α-pinene photooxidation. *Atmos. Environ.* **2024**, *337*, No. 120778.

(19) Zhao, Y.; Zhang, Z.; Zhao, Y.; Wang, C.; Xie, H.; Yang, J.; Zhang, W.; Wu, G.; Li, G.; Jiang, L.; Yang, X. Comparative studies of the NO_x impacts on the photooxidation mechanisms of isomeric monoterpenes of β-pinene and limonene. *J. Environ. Sci.* **2025**, *158*, 337−350.

(20) Zhao, Y.; Wang, C.; Zhao, Y.; Shao, Y.; Xie, H.; Yang, J.; Zhang, W.; Wu, G.; Li, G.; Jiang, L.; Yang, X. Anthropogenic effects on Δ^3-carene photooxidation: Different oxidants induce significant changes of secondary organic aerosol formation mechanisms. *Atmos. Environ.* **2025**, *357*, No. 121313.

(21) Chen, T. Z.; Zhang, P.; Chu, B. W.; Ma, Q. X.; Ge, Y. L.; He, H. Synergistic effects of SO_2 and NH_3 coexistence on SOA formation from gasoline evaporative emissions. *Environ. Sci. Technol.* **2023**, *57*, 6616−6625.

(22) Xu, L.; Yang, Z.; Tsona, N. T.; Wang, X.; George, C.; Du, L. Anthropogenic-biogenic interactions at night: Enhanced formation of secondary aerosols and particulate nitrogen-and sulfur-containing organics from β-pinene oxidation. *Environ. Sci. Technol.* **2021**, *55*, 7794−7807.

(23) Du, L.; Xu, L.; Li, K.; George, C.; Ge, M. NH_3 weakens the enhancing effect of SO_2 on biogenic secondary organic aerosol formation. *Environ. Sci. Technol. Lett.* **2023**, *10*, 145−151.

(24) Zhang, Z.; Zhao, Y.; Zhao, Y.; Zang, X.; Xie, H.; Yang, J.; Zhang, W.; Wu, G.; Li, G.; Yang, X.; Jiang, L. Effects of NO and SO_2 on the secondary organic aerosol formation from isoprene photooxidation. *Atmos. Environ.* **2024**, *318*, No. 120248.

(25) Sipilä, M.; Berndt, T.; Petäjä, T.; Brus, D.; Vanhanen, J.; Stratmann, F.; Patokoski, J.; Mauldin, R. L.; Hyvärinen, A. P.; Lihavainen, H.; Kulmala, M. The role of sulfuric acid in atmospheric nucleation. *Science* **2010**, *327*, 1243−1246.

(26) Zhou, S.; Guo, F.; Chao, C.-Y.; Yoon, S.; Alvarez, S. L.; Shrestha, S.; Flynn, J. H., III; Usenko, S.; Sheesley, R. J.; Griffin, R. J. Marine submicron aerosols from the Gulf of Mexico: Polluted and acidic with rapid production of sulfate and organosulfates. *Environ. Sci. Technol.* **2023**, *57*, 5149−5159.

(27) Stangl, C. M.; Krasnomowitz, J. M.; Apsokardu, M. J.; Tiszenkel, L.; Ouyang, Q.; Lee, S.; Johnston, M. V. Sulfur dioxide modifies aerosol particle formation and growth by ozonolysis of monoterpenes and isoprene. *J. Geophys. Res. Atmos.* **2019**, *124*, 4800−4811.

(28) Yang, Z.; Li, K.; Tsona, N. T.; Luo, X.; Du, L. SO_2 enhances aerosol formation from anthropogenic volatile organic compound ozonolysis by producing sulfur-containing compounds. *Atmos. Chem. Phys.* **2023**, *23*, 417−430.

(29) Atkinson, R.; Arey, J. Atmospheric degradation of volatile organic compounds. *Chem. Rev.* **2003**, *103*, 4605−4638.

(30) Kesselmeier, J.; Kuhn, U.; Wolf, A.; Andreae, M. O.; Ciccioli, P.; Brancaleoni, E.; Frattoni, M.; Guenther, A.; Greenberg, J.; De Castro Vasconcellos, P.; de Oliva, T.; Tavares, T.; Artaxo, P. Atmospheric volatile organic compounds (VOC) at a remote tropical forest site in central Amazonia. *Atmos. Environ.* **2000**, *34*, 4063−4072.

(31) Jardine, A. B.; Jardine, K. J.; Fuentes, J. D.; Martin, S. T.; Martins, G.; Durgante, F.; Carneiro, V.; Higuchi, N.; Manzi, A. O.; Chambers, J.

https://doi.org/10.1021/acs.est.5c10374
Environ. Sci. Technol. 2026, 60, 5097−5108

Q. Highly reactive light-dependent monoterpenes in the Amazon. *Geophys. Res. Lett.* **2015**, *42*, 1576−1583.
(32) Ahlberg, E.; Falk, J.; Eriksson, A.; Holst, T.; Brune, W. H.; Kristensson, A.; Roldin, P.; Svenningsson, B. Secondary organic aerosol from VOC mixtures in an oxidation flow reactor. *Atmos. Environ.* **2017**, *161*, 210−220.
(33) Gu, S.; Khalaj, F.; Perraud, V.; Faiola, C. L. Emerging investigator series: secondary organic aerosol formation from photooxidation of acyclic terpenes in an oxidation flow reactor. *Environ. Sci. Processes Impacts* **2024**, *26*, 1156−1170.
(34) Tan, Z. F.; Hantschke, L.; Kaminski, M.; Acir, I. H.; Bohn, B.; Cho, C. M.; Dorn, H. P.; Li, X.; Novelli, A.; Nehr, S.; Rohrer, F.; Tillmann, R.; Wegener, R.; Hofzumahaus, A.; Kiendler-Scharr, A.; Wahner, A.; Fuchs, H. Atmospheric photo-oxidation of myrcene: OH reaction rate constant, gas-phase oxidation products and radical budgets. *Atmos. Chem. Phys.* **2021**, *21*, 16067−16091.
(35) Deng, P.; Wang, L. Y.; Wang, L. M. Mechanism of gas-phase ozonolysis of β-myrcene in the atmosphere. *J. Phys. Chem. A* **2018**, *122*, 3013−3020.
(36) Liu, S.; Galeazzo, T.; Valorso, R.; Shiraiwa, M.; Faiola, C. L.; Nizkorodov, S. A. Secondary organic aerosol from OH-initiated oxidation of mixtures of *d*-limonene and β-myrcene. *Environ. Sci. Technol.* **2024**, *58*, 13391−13401.
(37) Zang, X.; Zhang, Z.; Zhao, Y.; Li, G.; Xie, H.; Zhang, W.; Wu, G.; Yang, X.; Jiang, L. Effects of NO_2 and SO_2 on the secondary organic aerosol formation from β-pinene photooxidation. *J. Environ. Sci.* **2024**, *136*, 151−160.
(38) Zang, X.; Zhang, Z.; Jiang, S.; Zhao, Y.; Wang, T.; Wang, C.; Li, G.; Xie, H.; Yang, J.; Wu, G.; Zhang, W.; Shu, J.; Fan, H.; Yang, X.; Jiang, L. Aerosol mass spectrometry of neutral species based on a tunable vacuum ultraviolet free electron laser. *Phys. Chem. Chem. Phys.* **2022**, *24*, 16484−16492.
(39) Normile, D. Unique free electron laser laboratory opens in China. *Science* **2017**, *355*, 235.
(40) DeCarlo, P. F.; Kimmel, J. R.; Trimborn, A.; Northway, M. J.; Jayne, J. T.; Aiken, A. C.; Gonin, M.; Fuhrer, K.; Horvath, T.; Docherty, K. S.; Worsnop, D. R.; Jimenez, J. L. Field-deployable, high-resolution, time-of-flight aerosol mass spectrometer. *Anal. Chem.* **2006**, *78*, 8281−8289.
(41) Ng, N. L.; Canagaratna, M. R.; Zhang, Q.; Jimenez, J. L.; Tian, J.; Ulbrich, I. M.; Kroll, J. H.; Docherty, K. S.; Chhabra, P. S.; Bahreini, R.; Murphy, S. M.; Seinfeld, J. H.; Hildebrandt, L.; Donahue, N. M.; DeCarlo, P. F.; Lanz, V. A.; Prévôt, A. S. H.; Dinar, E.; Rudich, Y.; Worsnop, D. R. Organic aerosol components observed in Northern Hemispheric datasets from aerosol mass spectrometry. *Atmos. Chem. Phys.* **2010**, *10*, 4625−4641.
(42) Aiken, A. C.; Decarlo, P. F.; Kroll, J. H.; Worsnop, D. R.; Huffman, J. A.; Docherty, K. S.; Ulbrich, I. M.; Mohr, C.; Kimmel, J. R.; Sueper, D.; Sun, Y.; Zhang, Q.; Trimborn, A.; Northway, M.; Ziemann, P. J.; Canagaratna, M. R.; Onasch, T. B.; Alfarra, M. R.; Prevot, A. S. H.; Dommen, J.; Duplissy, J.; Metzger, A.; Baltensperger, U.; Jimenez, J. L. O/C and OM/OC ratios of primary, secondary, and ambient organic aerosols with high-resolution time-of-flight aerosol mass spectrometry. *Environ. Sci. Technol.* **2008**, *42*, 4478−4485.
(43) Ng, N. L.; Canagaratna, M. R.; Jimenez, J. L.; Chhabra, P. S.; Seinfeld, J. H.; Worsnop, D. R. Changes in organic aerosol composition with aging inferred from aerosol mass spectra. *Atmos. Chem. Phys.* **2011**, *11*, 6465−6474.
(44) Canagaratna, M. R.; Jimenez, J. L.; Kroll, J. H.; Chen, Q.; Kessler, S. H.; Massoli, P.; Hildebrandt Ruiz, L.; Fortner, E.; Williams, L. R.; Wilson, K. R.; Surratt, J. D.; Donahue, N. M.; Jayne, J. T.; Worsnop, D. R. Elemental ratio measurements of organic compounds using aerosol mass spectrometry: Characterization, improved calibration, and implications. *Atmos. Chem. Phys.* **2015**, *15*, 253−272.
(45) Frisch, M. J.; Trucks, G. W.; Schlegel, H. B.; Scuseria, G. E.; Robb, M. A.; Cheeseman, J. R.; Scalmani, G.; Barone, V.; Petersson, G. A.; Nakatsuji, H.; Li, X.; Caricato, M.; Marenich, A. V.; Bloino, J.; Janesko, B. G.; Gomperts, R.; Mennucci, B.; Hratchian, H. P.; Ortiz, J. V.; Izmaylov, A. F.; Sonnenberg, J. L.; Williams-Young, D.; Ding, F.; Lipparini, F.; Egidi, F.; Goings, J.; Peng, B.; Petrone, A.; Henderson, T.; Ranasinghe, D.; Zakrzewski, V. G.; Gao, J.; Rega, N.; Zheng, G.; Liang, W.; Hada, M.; Ehara, M.; Toyota, K.; Fukuda, R.; Hasegawa, J.; Ishida, M.; Nakajima, T.; Honda, Y.; Kitao, O.; Nakai, H.; Vreven, T.; Throssell, K.; J. A. Montgomery, J.; Peralta, J. E.; Ogliaro, F.; Bearpark, M. J.; Heyd, J. J.; Brothers, E. N.; Kudin, K. N.; Staroverov, V. N.; Keith, T. A.; Kobayashi, R.; Normand, J.; Raghavachari, K.; Rendell, A. P.; Burant, J. C.; Iyengar, S. S.; Tomasi, J.; Cossi, M.; Millam, J. M.; Klene, M.; Adamo, C.; Cammi, R.; Ochterski, J. W.; Martin, R. L.; Morokuma, K.; Farkas, O.; Foresman, J. B.; Fox, D. J.; *Gaussian 16*, Revision B.01; Gaussian, Inc.: Wallingford, CT, USA, **2016**.
(46) Zhang, Z.; Zhao, Y.; Zhao, Y.; Zang, X.; Xie, H.; Yang, J.; Zhang, W.; Wu, G.; Li, G.; Yang, X.; Jiang, L. Effects of isoprene on the ozonolysis of Δ^3-carene and β-caryophyllene: Mechanisms of secondary organic aerosol formation and cross-dimerization. *J. Environ. Sci.* **2025**, *150*, 556−570.
(47) Zhao, Y.; Zhao, Y.; Wang, C.; Shao, Y.; Xie, H.; Yang, J.; Zhang, W.; Wu, G.; Li, G.; Jiang, L.; Yang, X. Photooxidation and ozonolysis of α-pinene and limonene mixtures: Mechanisms of secondary organic aerosol formation and cross-dimerization. *J. Environ. Sci.* **2026**, *161*, 525−535.
(48) Perring, A.; Pusede, S.; Cohen, R. C. An observational perspective on the atmospheric impacts of alkyl and multifunctional nitrates on ozone and secondary organic aerosol. *Chem. Rev.* **2013**, *113*, 5848−5870.
(49) Orlando, J. J.; Tyndall, G. S. Laboratory studies of organic peroxy radical chemistry: An overview with emphasis on recent issues of atmospheric significance. *Chem. Soc. Rev.* **2012**, *41*, 6294−6317.
(50) Lim, Y. B.; Ziemann, P. J. Products and mechanism of secondary organic aerosol formation from reactions of n-alkanes with OH radicals in the presence of NO_x. *Environ. Sci. Technol.* **2005**, *39*, 9229−9236.
(51) Capouet, M.; Müller, J.-F. A group contribution method for estimating the vapour pressures of α-pinene oxidation products. *Atmos. Chem. Phys.* **2006**, *6*, 1455−1467.
(52) Wang, D. S.; Masoud, C. G.; Modi, M.; Hildebrandt Ruiz, L. Isoprene-chlorine oxidation in the presence of NO and implications for urban atmospheric chemistry. *Environ. Sci. Technol.* **2022**, *56*, 9251−9264.
(53) Eddingsaas, N. C.; Loza, C. L.; Yee, L. D.; Seinfeld, J. H.; Wennberg, P. O. α-Pinene photooxidation under controlled chemical conditions - Part 1: Gas-phase composition in low- and high-NO environments. *Atmos. Chem. Phys.* **2012**, *12*, 6489−6504.
(54) Ye, J. H.; Abbatt, J. P. D.; Chan, A. W. H. Novel pathway of SO_2 oxidation in the atmosphere: reactions with monoterpene ozonolysis intermediates and secondary organic aerosol. *Atmos. Chem. Phys.* **2018**, *18*, 5549−5565.
(55) Kürten, A.; Münch, S.; Rondo, L.; Bianchi, F.; Duplissy, J.; Jokinen, T.; Junninen, H.; Sarnela, N.; Schobesberger, S.; Simon, M.; Sipilä, M.; Almeida, J.; Amorim, A.; Dommen, J.; Donahue, N. M.; Dunne, E. M.; Flagan, R. C.; Franchin, A.; Kirkby, J.; Kupc, A.; Makhmutov, V.; Petäjä, T.; Praplan, A. P.; Riccobono, F.; Steiner, G.; Tomé, A.; Tsagkogeorgas, G.; Wagner, P. E.; Wimmer, D.; Baltensperger, U.; Kulmala, M.; Worsnop, D. R.; Curtius, J. Thermodynamics of the formation of sulfuric acid dimers in the binary (H_2SO_4-H_2O) and ternary (H_2SO_4-H_2O-NH_3) system. *Atmos. Chem. Phys.* **2015**, *15*, 10701−10721.
(56) Kroll, J. H.; Donahue, N. M.; Jimenez, J. L.; Kessler, S. H.; Canagaratna, M. R.; Wilson, K. R.; Altieri, K. E.; Mazzoleni, L. R.; Wozniak, A. S.; Bluhm, H.; Mysak, E. R.; Smith, J. D.; Kolb, C. E.; Worsnop, D. R. Carbon oxidation state as a metric for describing the chemistry of atmospheric organic aerosol. *Nat. Chem.* **2011**, *3*, 133−139.
(57) Li, Y.; Bai, B.; Dykema, J.; Shin, N.; Lambe, A. T.; Chen, Q.; Kuwata, M.; Ng, N. L.; Keutsch, F. N.; Liu, P. Predicting real refractive index of organic aerosols from elemental composition. *Geophys. Res. Lett.* **2023**, *50*, No. e2023GL103446.
(58) Heald, C. L.; Kroll, J. H.; Jimenez, J. L.; Docherty, K. S.; DeCarlo, P. F.; Aiken, A. C.; Chen, Q.; Martin, S. T.; Farmer, D. K.; Artaxo, P. A

https://doi.org/10.1021/acs.est.5c10374
Environ. Sci. Technol. 2026, 60, 5097−5108

simplified description of the evolution of organic aerosol composition in the atmosphere. *Geophys. Res. Lett.* **2010**, *37*, No. L08803.
(59) Romonosky, D. E.; Laskin, A.; Laskin, J.; Nizkorodov, S. A. High-resolution mass spectrometry and molecular characterization of aqueous photochemistry products of common types of secondary organic aerosols. *J. Phys. Chem. A* **2015**, *119*, 2594−2606.
(60) Zhao, Y. Y.; Bai, J.; Zhang, C. X.; Gong, C.; Sun, X. M. Theoretical study on the chemical formation mechanism of a β-myrcene ozonolysis reaction under atmospheric conditions. *Can. J. Chem.* **2012**, *90*, 708−715.
(61) Peeters, J.; Boullart, W.; Pultau, V.; Vandenberk, S.; Vereecken, L. Structure-activity relationship for the addition of OH to (poly)-alkenes: Site-specific and total rate constants. *J. Phys. Chem. A* **2007**, *111*, 1618−1631.
(62) Reissell, A.; Aschmann, S. M.; Atkinson, R.; Arey, J. Products of the OH radical- and O_3-nitiated reactions of myrcene and ocimene. *J. Geophys. Res. Atmos.* **2002**, *107*, 4138.
(63) Böge, O.; Mutzel, A.; Iinuma, Y.; Yli-Pirilä, P.; Kahnt, A.; Joutsensaari, J.; Herrmann, H. Gas-phase products and secondary organic aerosol formation from the ozonolysis and photooxidation of myrcene. *Atmos. Environ.* **2013**, *79*, 553−560.
(64) Lee, A.; Goldstein, A. H.; Keywood, M. D.; Gao, S.; Varutbangkul, V.; Bahreini, R.; Ng, N. L.; Flagan, R. C.; Seinfeld, J. H. Gas-phase products and secondary aerosol yields from the ozonolysis of ten different terpenes. *J. Geophys. Res. Atmos.* **2006**, *111*, No. D07302.
(65) Zhao, Y.; Thornton, J. A.; Pye, H. O. T. Quantitative constraints on autoxidation and dimer formation from direct probing of monoterpene-derived peroxy radical chemistry. *Proc. Natl. Acad. Sci. U.S.A.* **2018**, *115*, 12142−12147.
(66) Song, X. L.; Lin, X. X.; Xia, Y.; Ma, Z. J.; Jin, L. Q.; Zhang, W. J.; Wang, Z. D.; Fittschen, C.; Tang, X. F. Product and mechanistic insights into the ozonolysis of Δ^3-carene. *Atmos. Environ.* **2025**, *360*, No. 121449.
(67) Yue, H.; Zhang, C. H.; Lin, X. X.; Wen, Z. Y.; Zhang, W. J.; Mostafa, S.; Luo, P. L.; Zhang, Z. H.; Hemberger, P.; Fittschen, C.; Tang, X. F. Dimeric product of peroxy radical self-reaction probed with VUV photoionization mass spectrometry and theoretical calculations: The case of $C_2H_5OOC_2H_5$. *Int. J. Mol. Sci.* **2023**, *24*, 3731.
(68) Wyche, K. P.; Monks, P. S.; Smallbone, K. L.; Hamilton, J. F.; Alfarra, M. R.; Rickard, A. R.; McFiggans, G. B.; Jenkin, M. E.; Bloss, W. J.; Ryan, A. C.; Hewitt, C. N.; MacKenzie, A. R. Mapping gas-phase organic reactivity and concomitant secondary organic aerosol formation: chemometric dimension reduction techniques for the deconvolution of complex atmospheric data sets. *Atmos. Chem. Phys.* **2015**, *15*, 8077−8100.
(69) Kim, D.; Stevens, P. S.; Hites, R. A. Rate constants for the gas-phase reactions of OH and O_3 with β-ocimene, β-myrcene, and α-and β-farnesene as a function of temperature. *J. Phys. Chem. A* **2011**, *115*, 500−506.
(70) Berndt, T.; Scholz, W.; Mentler, B.; Fischer, L.; Herrmann, H.; Kulmala, M.; Hansel, A. Accretion product formation from self- and cross-reactions of RO_2 radicals in the atmosphere. *Angew. Chem., Int. Ed.* **2018**, *57*, 3820−3824.
(71) Shallcross, D.; Teresaraventosduran, M.; Bardwell, M.; Bacak, A.; Solman, Z.; PErcival, C. A semi-empirical correlation for the rate coefficients for cross- and self-reactions of peroxy radicals in the gas-phase. *Atmos. Environ.* **2005**, *39*, 763−771.
(72) Surratt, J. D.; Kroll, J. H.; Kleindienst, T. E.; Edney, E. O.; Claeys, M.; Sorooshian, A.; Ng, N. L.; Offenberg, J. H.; Lewandowski, M.; Jaoui, M.; Flagan, R. C.; Seinfeld, J. H. Evidence for organosulfates in secondary organic aerosol. *Environ. Sci. Technol.* **2007**, *41*, 517−527.
(73) Berndt, T.; Richters, S.; Jokinen, T.; Hyttinen, N.; Kurtén, T.; Otkjær, R. V.; Kjaergaard, H. G.; Stratmann, F.; Herrmann, H.; Sipilä, M.; Kulmala, M.; Ehn, M. Hydroxyl radical-induced formation of highly oxidized organic compounds. *Nat. Commun.* **2016**, *7*, 13677.
(74) Chen, T.; Zhang, P.; Chu, B.; Ma, Q.; Ge, Y.; Liu, J.; He, H. Secondary organic aerosol formation from mixed volatile organic compounds: Effect of RO_2 chemistry and precursor concentration. *npj Clim. Atmos. Sci.* **2022**, *5*, 95.
(75) Bates, K. H.; Burke, G. J. P.; Cope, J. D.; Nguyen, T. B. Secondary organic aerosol and organic nitrogen yields from the nitrate radical (NO_3) oxidation of alpha-pinene from various RO_2 fates. *Atmos. Chem. Phys.* **2022**, *22*, 1467−1482.
(76) Wang, S. Y.; Zhou, S. M.; Tao, Y.; Tsui, W. G.; Ye, J. H.; Yu, J. Z.; Murphy, J. G.; McNeill, V. F.; Abbatt, J. P. D.; Chan, A. W. H. Organic peroxides and sulfur dioxide in aerosol: Source of particulate sulfate. *Environ. Sci. Technol.* **2019**, *53*, 10695−10704.
(77) Jang, M. S.; Czoschke, N. M.; Lee, S.; Kamens, R. M. Heterogeneous atmospheric aerosol production by acid-catalyzed particle-phase reactions. *Science* **2002**, *298*, 814−817.
(78) Massoli, P.; Stark, H.; Canagaratna, M. R.; Krechmer, J. E.; Xu, L.; Ng, N. L.; Mauldin, R. L.; Yan, C.; Kimmel, J.; Misztal, P. K.; Jimenez, J. L.; Jayne, J. T.; Worsnop, D. R. Ambient measurements of highly oxidized gas-phase molecules during the Southern Oxidant and Aerosol Study (SOAS) 2013. *Acs Earth Space Chem.* **2018**, *2*, 653−672.
(79) Le Breton, M.; Wang, Y. J.; Hallquist, Å. M.; Pathak, R. K.; Zheng, J.; Yang, Y. D.; Shang, D. J.; Glasius, M.; Bannan, T. J.; Liu, Q. Y.; Chan, C. K.; Percival, C. J.; Zhu, W. F.; Lou, S. R.; Topping, D.; Wang, Y. C.; Yu, J. Z.; Lu, K. D.; Guo, S.; Hu, M.; Hallquist, M. Online gas- and particle-phase measurements of organosulfates, organosulfonates and nitrooxy organosulfates in Beijing utilizing a FIGAERO ToF-CIMS. *Atmos. Chem. Phys.* **2018**, *18*, 10355−10371.
(80) Friedman, B.; Brophy, P.; Brune, W. H.; Farmer, D. K. Anthropogenic sulfur perturbations on biogenic oxidation: SO_2 additions impact gas-phase OH oxidation products of α- and β-pinene. *Environ. Sci. Technol.* **2016**, *50*, 1269−1279.
(81) Sun, H. W.; Liu, Y. L.; Nie, W.; Li, Y. Y.; Ge, D. F.; Xu, T.; Yin, J. C.; Liu, C.; Fu, Z. H.; Qi, X. M.; Liu, T. Y.; Zha, Q. Z.; Yan, C.; Wang, Z.; Chi, X. G.; Ding, A. J. Unexpected gas-phase formation of glycolic acid sulfate in the atmosphere. *Environ. Sci. Technol.* **2025**, *59*, 16556−16566.

https://doi.org/10.1021/acs.est.5c10374
Environ. Sci. Technol. 2026, 60, 5097−5108